IEEE Access
Multidisciplinary | Rapid Review | Open Access Journal

Received 25 July 2022, accepted 22 August 2022, date of publication 26 August 2022, date of current version 2 September 2022.

Digital Object Identifier 10.1109/ACCESS.2022.3202296

RESEARCH ARTICLE

Research on Novel Hybrid Torque Sharing Function for Switched Reluctance Motors

FAHAD AL-AMYAL AND LÁSZLÓ SZÁMEL
Department of Electric Power Engineering, Faculty of Electrical Engineering and Informatics, Budapest University of Technology and Economics, 1111 Budapest, Hungary

Corresponding author: Fahad Al-Amyal (fahad.alamyal@edu.bme.hu)

ABSTRACT Torque Sharing Function (TSF) approach can be considered a promising method to solve the torque ripple issue in switched reluctance motors (SRMs) drives at low and medium speed ranges. However, at the high-speed operation of the machine, the actual phase current fails to track the reference current profile. This limitation primarily occurs over the demagnetization period of each phase current. Consequently, each phase torque will also fail to track its corresponding reference torque created by the TSF strategy. As a result of the torque tracking error, a considerable torque ripple will be produced. To address this issue, a novel hybrid TSF is proposed in this research article. The hybrid TSF can adapt during the real-time operation relying on the current (and thus the torque) tracking capability during the magnetization period, which is much higher than during the demagnetization period. At each electrical cycle, the rising part of the incoming phase torque reference is re-profiled to mirror the declining part of the actual torque of the outgoing phases. And therefore, the torque tracking error can be compensated, and a remarkable torque ripple suppression will be attained. Additionally, within the hybrid TSF, an overlap angle controller is also proposed in this work and participated in high-speed operation. The controller keeps monitoring the error between the commanded torque and the actual average torque of the machine, and by adjusting the overlap angle in real-time, the error can be further compensated. Thus, further torque tracking capability is attained. A set of simulation results are presented and favorably compared with other traditional TSF approaches to demonstrate the feasibility and validity of the proposed hybrid TSF.

INDEX TERMS Switched reluctance motor, hybrid torque sharing function, indirect instantaneous torque control.

I. INTRODUCTION

Compared to other types of electrical motors, switched reluctance motors (SRMs) can provide lower cost, greater efficiency, and a fault-tolerant drive. This is because SRMs have no permanent magnets in their structure or winding in their rotary parts. They can generate high electromagnetic torque relying on the tendency of their salient rotor poles to align with magnetized stator poles to attain minimum reluctance (or maximum inductance). However, owing to their highly nonlinear inductance/torque characteristics and the discrete excitation mechanisms, SRMs encounter undesirable ripples in their output torque. They also suffer from other drawbacks, including acoustic noise, low power and torque densities, and difficulty obtaining accurate modeling. These weaknesses are the major limitations against the wider employment of SRMs in the present technology [1], [2], [3], [4], [5], [6], [7], [8].

Recently, engineers focused on solving the problem of torque ripple of SRMs and maximizing their performance by proposing different strategies which can be assorted within two main headings, including machine structure optimization and advanced control systems. Although machine structure optimization can lead to torque ripple suppression and boost the machine performance, it can only do so to a certain extent [9], [10], [11], [12], [13], [14]. Moreover, adjusting the dimensions of an already manufactured machine is challenging.

The control systems, on the other hand, have the potential to significantly reduce torque ripple and maximize the performance of SRMs [15], [16], [17], [18], [19]. The commonly utilized control schemes in the literature are the traditional

The associate editor coordinating the review of this manuscript and approving it for publication was Christopher H. T. Lee.

current control (CC) systems [20], [21], [22], [23], [24], [25] and the advanced torque control (TC) systems. The TC systems mainly include the average (ATC) [26], [27], [28], [29], [30] and the instantaneous torque control (ITC) systems. Although these control systems succeeded in providing remarkable torque ripple suppression and improving other aspects of SRM performance, there are still some drawbacks to each. For instance, while the CC and the ATC systems provide an efficient, wide speed range and low-cost control drives, the output torque has a considerable ripple. Because in the CC and the ATC systems, the current in each phase of the machine can only be regulated in a form of square signals, and no current profiling is possible. Consequently, torque ripple minimization can only be achieved partially by optimizing the excitation parameters (turn-on and turn-off angles) for a specified reference current. Alternatively, the ITC systems can heavily suppress the torque ripple because, within these systems, the output torque is regulated instantaneously at each sample point of the rotor position. Consequently, optimum profiling of the phase currents will be realized; therefore, smooth output torque will be generated but only to limited speed ranges. Because in the high-speed operation of the SRM, it's challenging to track a reference current signal with profiled shape in a short excitation time. The ITC systems can be categorized under direct (DITC) [31], [32], [33], [34], [35] and indirect (IITC) instantaneous control systems [36], [37], [38], [39], [40], [41], [42]. In the DITC system, the out torque of the machine is estimated, compared with a reference torque value, and regulated directly via a torque controller. In contrast, in the IITC, the reference torque is partitioned between the motor phases through an intelligent torque sharing function (TSF). Each phase torque is then reversed to its corresponding current reference profile, and then by tracking the obtained current using a current controller, the reference torque can be regulated indirectly.

In [31], an optimized DITC system is implemented. A mathematical expression for the switch-on angle is employed to obtain maximized torque/ampere ratio. While the switch-off angle is defined via solving an optimization problem, the objective of this problem is to attain the lowest torque ripples with the highest machine efficiency. In [32], both hysteresis and PWM techniques are involved in performing a modified DITC. With this modification, the torque profile of the SRM is highly improved. In [33], a novel real-time commutation strategy is proposed to implement an enhanced DITC system. The turn-on angle is adjusted at each electrical cycle to reduce the error magnitude between the commanded and the actual torque. On the other hand, the turn-off angle is modified on-line to prevent negative torque generation and improve the torque/ampere ratio. [34] proposes a new switching strategy within the DITC system to attain a minimized torque ripple and improved torque/ampere ratio. In [35], a DITC system with a fixed switching frequency is proposed by utilizing a PWM. Based on the torque characteristic, the rotor sector is reclassified, the PWM output signal, and the coefficients of the duty cycle are calculated to acquire torque ripple minimization and improved efficiency.

In [36], within different TSFs, the switch-on and the overlap angles are optimized using a genetic algorithm. This optimization problem aims to achieve torque ripple and copper loss reduction in wide-ranging speed operation of the SRMs. In [37], off-line TSF is proposed to meet three criteria: torque ripple and copper loss reduction and minimization of the rate of change of flux linkage. Minimizing the rate of change of flux linkage will result in a wider speed range operation of the machine. In [38], a novel IITC system is introduced, and optimum profiling of the phase current is implemented to enhance the machine's torque profile and reduce the copper losses. In [39], each phase current profile is first created from the torque reference using off-line computations and as well from the response of the phase current, which can be determined from the SRM dynamic model. Then, by formulating an optimization problem to shape the current command, the torque ripple and the copper losses are minimized, and the required average torque is maintained. In [40], each phase current is instantaneously modulated based on other phase currents to retain a reduced torque ripple. In [41], the turn-on and the overlap angles of a typical sinusoidal TSF are optimally selected based on a promoted ant colony algorithm. The focus is to suppress torque ripple, reduce the RMS value of the phase current, and provide the required average output torque at wide-ranged speed operation. The IITC is enhanced in [42]. The switch-on angle is primarily determined to attain maximum torque generation capability. The remaining error between the reference and motor torque is fed back to the TSF to achieve further error compensation. Thus, the torque ripple is minimized.

As a result of the lower inductance at the un-aligned rotor position, the current (and therefore, the torque) tracking capabilities of the rising portion of the incoming phase are much higher than in the declining part of the outgoing phase. This property is utilized beneficially to implement a novel hybrid TSF. The modification is done mainly at the overlap region between the adjusted motor phases. Where after estimating the behavior of the real phase torque during phase demagnetization. The rising part of the incoming reference torque is re-profiled in such a way to become the exact mirroring of the declining part of the real estimated torque of the outgoing phases. In this case, the torque tracking error during the demagnetization is handled indirectly by modifying the incoming phases' reference torque. Thus, constant torque is maintained with lowered torque ripple. Besides, this work also proposes an overlap angle controller within the hybrid TSF. The controller keeps monitoring the error between the commanded torque and the real generated average torque of the machine. By adjusting the overlap angle in real-time, the error can be compensated. Thus, further torque ripple minimization can be attained. This study employs a four-phase, 8/6 poles SRM motor prototype with rated parameters of 4 kW, 600 V, and 1500 r/min.

The article layout is as follows: section II illustrates the SRM modeling and the selected performance indices. The IITC system and the commonly utilized TSF in the literature are involved in section III. Sections IV and V explain the adopted hybrid TSF and the excitation system, respectively. A set of steady-state and dynamic simulations are presented and compared favorably with other TSF approaches in section VI. Finally, Section VII provides a brief conclusion to this article.

II. MACHINE MODELING

Owing to the salience structure of both stator and rotor poles of SRMs, the magnetic flux per phase $\lambda_{ph}(i_{ph}, \theta)$, inductance per phase $L_{ph}(i_{ph}, \theta)$, and the output torque $T(i_{ph}, \theta)$ are highly nonlinear against the phase current (i_{ph}) and the position of the rotor (θ). The voltage (v_{ph}) and the electromagnetic torque (T_{ph}) equations of one phase of the machine are depicted in (1) and (2), respectively. The machine's total output torque (T_e) can be obtained by summing the generated torque from all phases as indicated in (3). The mathematical expression of the mechanical dynamics of the SRM is depicted in (4).

$$v_{ph} = Ri_{ph} + \frac{\partial \lambda_{ph}(i_{ph}, \theta)}{\partial t} \tag{1}$$

$$T_{ph} = \frac{1}{2} i^2 \frac{\partial L_{ph}(\theta)}{\partial \theta} \tag{2}$$

$$T_e = \sum T_{ph} \tag{3}$$

$$T_e - T_L = B\omega + J\frac{d\omega}{dt} \tag{4}$$

where, T_L is the load torque, B and J are the frictional and inertia coefficients of the machine, and ω is the rotational speed.

The magnetic data of chosen 8/6 SRM prototype is obtained using the finite element method (FEM). These data are then experimentally validated so as to verify the accuracy of the adopted machine model [43]. The FEM obtained data of the magnetic flux linkage, inductance, and torque, along with their corresponding experimentally measured data, are shown in Fig. 1a, Fig. 1b, and Fig. 1c, respectively. For clarity and simplification, only a few curves are presented in these figures, but the complete data are determined in the entire current and position domains ($0 \leq i \leq 25$ A; $0° \leq \theta \leq 30°$) at a current and position steps of 0.25 A and 0.25° respectively. These data are then inserted in look-up tables and used in the Simulink model of the SRM. The fully unaligned and aligned rotor positions are expressed by the angles $\theta = 0°$ and $\theta = 30°$, respectively.

As depicted, a very good agreement is attained between the FEM-based and the experimentally based obtained data, and therefore, the machine model is verified for future simulation findings.

The performance of the machine will be evaluated according to different indices, including the average output torque (T_{ave}), the torque ripple percent (T_{ripple}), torque/ampere ratio (TAR), and the efficiency (η) of the machine. These indices

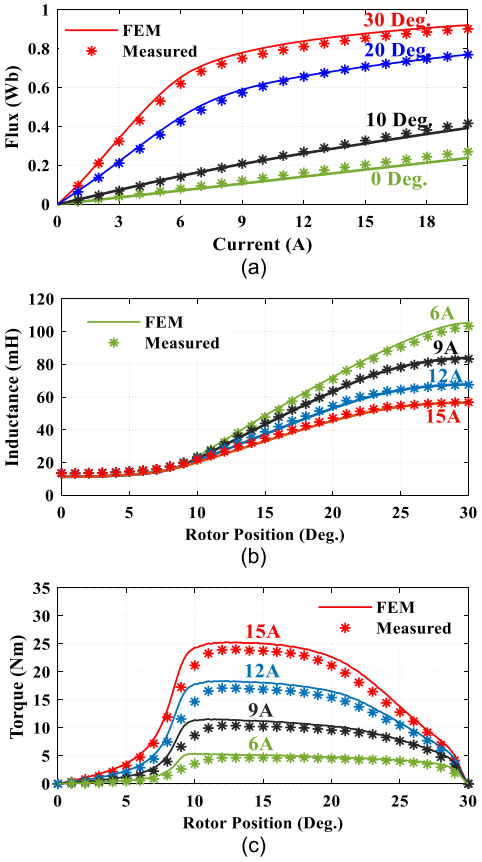

FIGURE 1. The FEM-based and the experimentally based magnetic characteristics of the chosen 8/6 SRM. (a) flux-linkage. (b) Inductance. (c) Torque.

can be obtained over one electrical cycle (τ) according to the following equations:

$$T_{ave} = \frac{1}{\tau}\int_0^{\tau} T_e\,(t)\,dt \tag{5}$$

$$T_{ripple} = \frac{T_{max} - T_{min}}{T_{ave}} \times 100\% \tag{6}$$

$$TAR = \frac{T_{ave}}{I_{RMS}} \tag{7}$$

$$\eta = \frac{\omega T_{ave}}{V_{dc} I_{ave}} \tag{8}$$

$$I_{ave} = \frac{1}{\tau}\int_0^{\tau} i_s\,(t)\,dt \tag{9}$$

where, I_{RMS} and I_{ave} are the RMS, and the average values of the supply current i_s, and V_{dc} is the dc supply voltage.

III. INDIRECT INSTANTANEOUS TORQUE CONTROL

The block diagram of the IITC system is depicted in Fig. 2. The output of the speed regulator is the commanded reference torque (T^*). The TSF then distributes T^* between the phases of the machine. Each k^{th} phase torque $T^*(k)$ signal is then reversed to its equivalent reference current signal (i^*). Then, using a current regulator, the phase current (i_{ph}) can track the obtained current signal, and thus the output torque of the SRM is regulated indirectly.

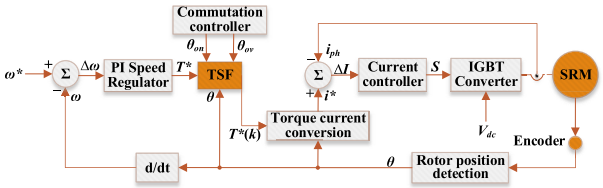

FIGURE 2. SRM drive based on IITC strategy.

The conventional TSF can be defined by using a mathematical expression to develop the dynamic behavior of each phase torque of the machine. In light of this, the reference torque of the k^{th} phase can be defined using (10).

$$T^*(k) = \begin{cases} 0 & 0 \le \theta < \theta_{on} \\ T^* f_{rise}(\theta) & \theta_{on} \le \theta < \theta_{on} + \theta_{ov} \\ T^* & \theta_{on} + \theta_{ov} \le \theta < \theta_{off} \\ T^* f_{dec}(\theta) & \theta_{off} \le \theta < \theta_{off} + \theta_{ov} \\ 0 & \theta_{off} + \theta_{ov} \le \theta < \theta_p \end{cases} \tag{10}$$

where, $T^*(k)$ is the torque reference assigned for phase k, $f_{rise}(\theta)$ is the rising (from zero to one) expression of the incoming phase torque reference, and $f_{dec}(\theta)$ is the declining (from one to zero) expression of the outgoing phase torque reference. The commonly used TSFs types are the linear and the nonlinear TFSs. The nonlinear TSFs include the sinusoidal and the exponential TSFs. Fig. 3a depicts a typical linear TSF, while in Fig. 3b, a typical nonlinear TSF based on sinusoidal formulation is presented.

The rising and the declining parts at the overlap region of the linear TSF can be formulated according to (11). While in the sinusoidal TSF, as in (12).

$$linear \begin{cases} f_{rise}(\theta) = \dfrac{1}{\theta_{ov}}(\theta - \theta_{on}) \\ f_{dec}(\theta) = 1 - \dfrac{1}{\theta_{ov}}\left(\theta - \theta_{off}\right) \end{cases} \tag{11}$$

$$sine \begin{cases} f_{rise}(\theta) = \dfrac{T^*}{2} - \dfrac{T^*}{2} cos \dfrac{\pi}{\theta_{ov}}(\theta - \theta_{on}) \\ f_{dec}(\theta) = \dfrac{T^*}{2} + \dfrac{T^*}{2} cos \dfrac{\pi}{\theta_{ov}}\left(\theta - \theta_{off}\right) \end{cases} \tag{12}$$

where, θ_{ov}, θ_{on}, and θ_{off} are the overlap, turn-on, and turn-off angles.

It is worth noting that these angles significantly impact the SRM performance. As a result, they should be selected carefully to attain maximized machine performance. However, for the selected four-phase SRM prototype, the rotor period (θ_p) is 60°; thus, the TSF is symmetrical about the rotor position of 15°. In light of this, the overlap angle and the turn-off angle must be selected according to (13) and (14), respectively [36].

$$\theta_{ov} \le 15° - \theta_{on} \tag{13}$$

$$\theta_{off} = \theta_{on} + 15° \tag{14}$$

The overlap angle limit indicated in (13) forces the outgoing phase torque reference to fully decay to zero before the aligned position (30°). Otherwise, if the overlap angle is selected beyond this limit, then the non-zero phase torque reference at the negative slop inductance zone (>30°) will generate a negative torque according to (2).

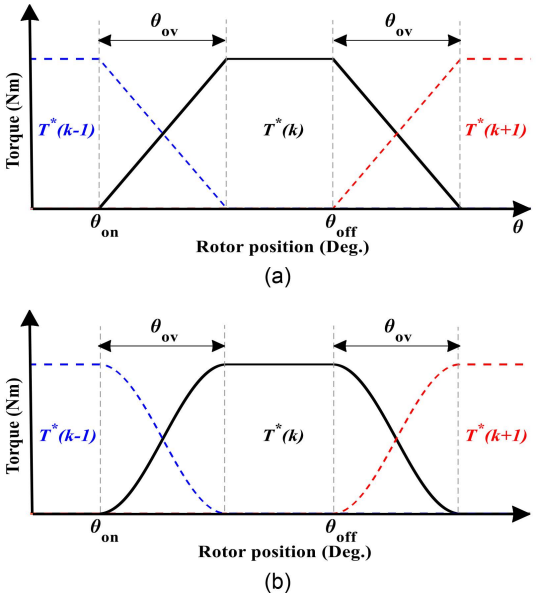

FIGURE 3. Typical TSF profiles. (a) Linear TSF. (b) sinusoidal TSF.

These parameters can be optimized off-line and stored in look-up tables or adjusted on-line during the real-time operation of the machine depending on specified criteria. Within the proposed IITC-based hybrid TSF, the turn-on and the overlap angles are adjusted during real-time operation to maximize the machine's torque-producing ability and improve the torque tracking accuracy, as illustrated in the next section.

IV. PROPOSED HYBRID TORQUE SHARING FUNCTION

Owing to the lower inductance at the un-aligned rotor position (Fig. 1b), the current and, therefore, the torque tracking capability of the rising incoming phase is much higher than in the declining outgoing phases. Fig. 4a shows a phase (k) reference current profile along with the actual phase current, while Fig. 4b shows the corresponding reference phase torque along with the actual torque when running the machine at a medium speed range.

Solving the (indicated by arrows) tracking error issues during phase demagnetization is challenging. However, it is still possible to improve the overall torque profile of the machine by re-profiling the rising part of the incoming phase torque $T^*(k+1)$ to become the exact mirroring of the real torque of the outgoing phase $T_e(k)$, as shown in Fig. 4b.

The solid black line corresponds to the torque reference of phase k, which is formed based on nonlinear TSF. The red line indicates the actual torque of phase k. The dotted black line corresponds to the torque reference of the previous (k-1) and the next (k+1) phases without a profiling strategy. And the indicated by pink line is the proposed phase torque reference for the next k+1 phase. As depicted by arrows in Fig. 4b, the pink line is re-profiled to the optimal shape in

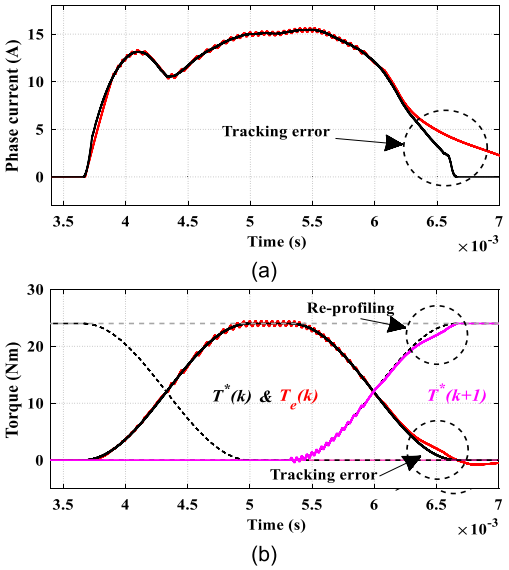

FIGURE 4. Tracking error during phase demagnetization. (a) Current tracking error. (b) Torque tracking error.

order to compensate the torque tracking error of the declining outgoing phase. In light of the previous, the hybrid TSF consists of two parts. The first part ($\theta_{on}+\theta_{ov} \leq \theta < \theta_{off}+\theta_{ov}$) is built off-line using mathematical formulation. The second part ($0 \leq \theta < \theta_{on}+\theta_{ov}$) is built on-line during machine operation in such a way to become the exact mirroring of the declining portion of the actual torque of the outgoing phases. Consequently, a constant torque level is maintained, and the torque ripple is kept minimal. The reference torque of phase k can be formulated based on hybrid TSF using (15).

$$T^*(k) = \begin{cases} 0 & 0 \leq \theta < \theta_{on} \\ T^* - T_e(k-1) & \theta_{on} \leq \theta < \theta_{on}+\theta_{ov} \\ T^* & \theta_{on}+\theta_{ov} \leq \theta < \theta_{off} \\ T^* f_{dec}(\theta) & \theta_{off} \leq \theta < \theta_{off}+\theta_{ov} \\ 0 & \theta_{off}+\theta_{ov} \leq \theta < \theta_p \end{cases} \quad (15)$$

where, $T_e(k\text{-}1)$ is the actual torque of the previous phase and is advanced by one sampling period, and the declining part $f_{dec}(\theta)$ of hybrid TSF can be formulated according to the linear or the nonlinear expression given in (11) and (12).

The compensation for the one sample delay for torque $T_e(k\text{-}1)$ is done by advancing its angle to be $(\theta+\omega T_s)$, where T_s is the sampling period, and it is equal to 100 μs for the outer loop speed controller, 20 μs for the current controller, and 2μs for the motor and the power converter.

V. PROPOSED EXCITATION SYSTEM

The timing of phase excitation has a significant impact on the SRM performance. As a result, the selection of the turn-on angle and, therefore, the corresponding turn-off angle (14) must be fulfilled carefully. For illustration, Fig. 5 depicts one phase current (I_{ph}) of SRM obtained using the traditional CC system and the inductance (L) of the same phase. These curves are plotted against the position of the rotor (θ).

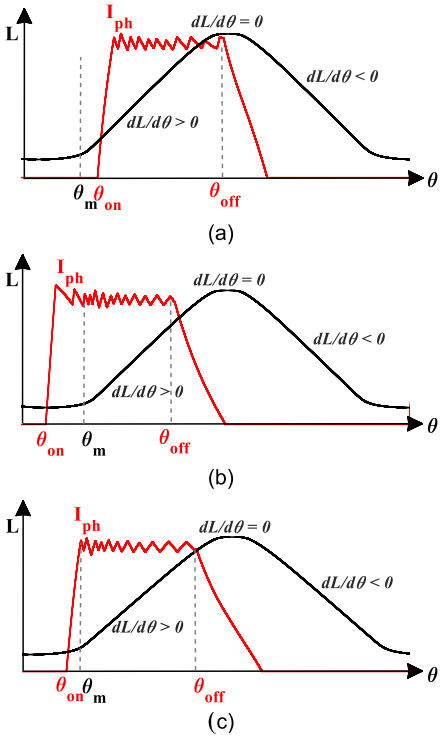

FIGURE 5. Different excitations methodologies for SRM. (a) Late excitation. (b) early excitation. (c) Optimal excitation.

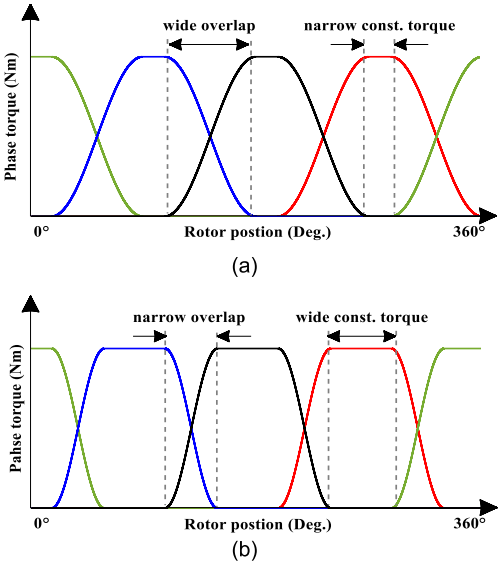

FIGURE 6. Sinusoidal TSF profile in different overlap angles. (a) wide overlap angle. (b) small overlap angle.

According to (2), to deliver a positive torque, the excitation of SRM phases must be applied during the positive slope zone ($dL/d\theta > 0$) of the inductance. Moreover, if a current is delivered to the phases during the fully unaligned or fully aligned rotor positions ($dL/d\theta \approx 0$), then a greater current will be demanded to generate the reference torque. In this case, the machine will operate with a lowered efficiency. In Fig. 5a, for instance, the phases are turned on too late after the rotor pole has already started overlapping (at θ_m) with the stator pole. In this case, the positive slope part before

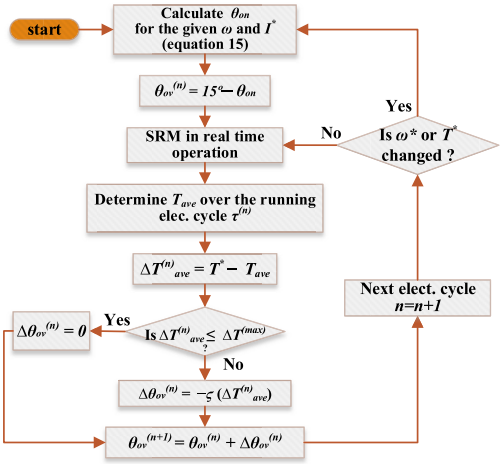

FIGURE 7. Flow chart for the adopted excitation strategy within the proposed IITC.

θ_{on} will not be employed for torque production. Alternately, in Fig. 5b, the phases are turned-on early before the overlapping at θ_m, and because of the low rate of change of the inductance between θ_{on} and θ_m, a higher current will be consumed for torque production. In light of this, for the best torque production capability, the turn-on angle can be selected in such a manner the current of each phase reaches its reference value exactly at θ_m, as depicted in Fig. 5c. This can be achieved using the following expression [44].

$$\theta_{on} = \theta_m - \frac{\omega L_u}{R + K_b\omega} ln\left[1 - I^*\left(\frac{R + K_b\omega}{V_{dc}}\right)\right] \quad (16)$$

where, L_u is the inductance per phase at the fully unaligned area, K_b is its derivative with respect to the rotor position, R is the resistance per phase, and I^* is the current reference.

The overlap angle θ_{ov}, also has a remarkable impact on the SRM performance, especially at high-speed operation. Fig. 6a and b show two TSFs profiles for the selected four-phase machine created using wide and small overlap angles. The advantage of using a wider angle is to provide slower rising and declining portions of the reference torque. Therefore, this will facilitate the torque tracking at the overlap zone and reduces the torque ripple. However, as the operation speed of the SRM increases, the excitation time of each phase will decrease. Accordingly, at a very high speed, the phase torque may fail to reach the constant reference torque value (T^*) in a very short time. And using a slow-rising portion as a commanded reference torque will be negatively reflected on the torque tracking capability over the entire excitation period. And in this case, the provided average torque of the machine (5) will decrease below T^*.

This paper proposes a controller for an optimal selection of the overlap angle. The controller is involved in the proposed IITC system to compensate for the error (ΔT_{ave}) between the commanded torque (T^*) and the actual average torque (T_{ave}) at high-speed operation. The overlap angle is set to its maximum limit at low and medium speed ranges, as indicated in (13), to ensure the best torque tracking accuracy. Above

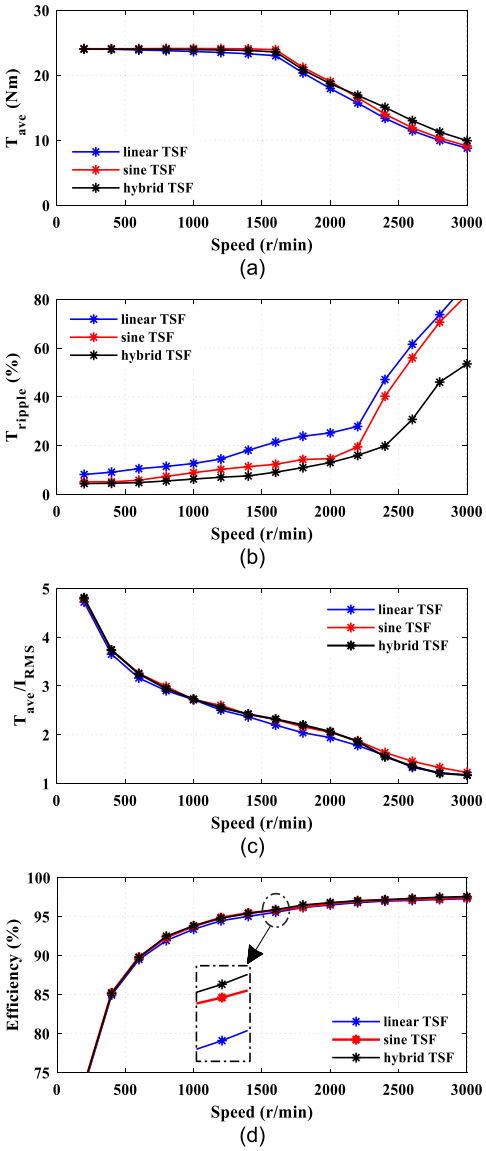

FIGURE 8. The steady-state obtained performance indices at a wide speed range of the SRM. (a) Average torque. (b) Torque ripple percent. (c) Torque/ampere ratio. (d) Efficiency.

the motor's base speed, the controller will keep monitoring the torque error in real-time operation within each electrical cycle. If the error given in (17) is acceptable (below a pre-specified tolerance), then no modification to the maximum initial angle is necessary.

$$\Delta T_{ave} = T^* - T_{ave} \quad (17)$$

On the other hand, if ΔT_{ave} is unacceptable, then a proper decrement ($-\Delta\theta_{ov}$) must be provided. As a result, a smaller overlap angle, narrower overlap region, and faster rising portion of the reference torque will be realized; therefore, higher average torque will be delivered. The overlap angle is continually updated at each electrical cycle until the desired torque error is attained or a pre-specified minimum angle is reached. The flowchart depicted in Fig. 7 illustrates the proposed excitation system.

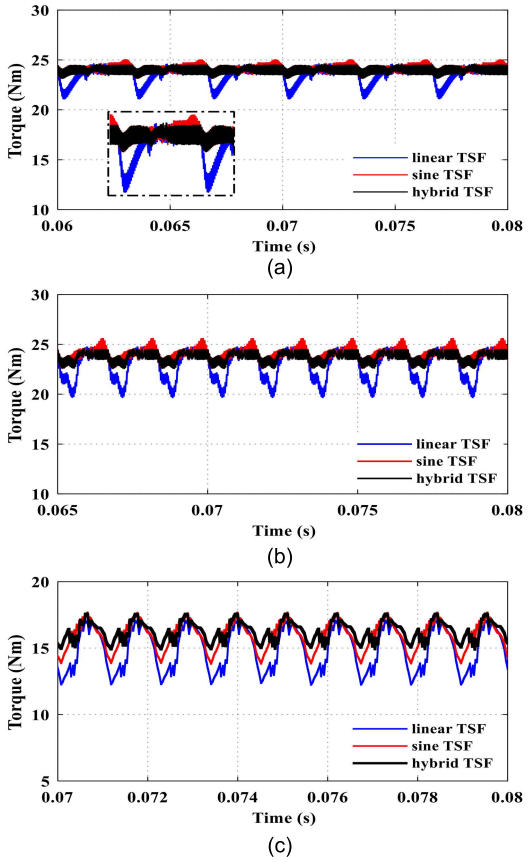

FIGURE 9. Torque profiles of the SRM at different operating points. (a) 750 r/min speed and 24 Nm torque. (b) 1500 r/min speed and 24 Nm torque. (c) 2250 r/min speed and 17 Nm torque.

TABLE 1. Parameters of the selected machine prototype.

Parameter	Values
Poles (stator/ rotor)	8/6
Power	4 kW
Rated current	9 A
Rated speed	1500 r/min
Resistance/ phase	0.642 Ω
Stator outer/ inner diameter	179.5/ 96.9 mm
Rotor outer/ shaft diameter	96.7 / 36 mm
Airgap /stack lengths	0.4 / 151 mm
Pole arcs (stator/ rotor)	20.45°/ 21.5°
No. of turns/ pole	88

The overlap angle decrement ($-\Delta\theta_{ov}$) is scaled according to the torque error (ΔT_{ave}) to provide faster angle modification in case if large torque error is detected. ς is a small scaling parameter.

VI. SIMULATION RESULTS

To verify the effectiveness of the proposed hybrid TSF, MATLAB simulations are carried out to present the steady-state and the dynamic performance of the SRM. A comparative analysis against the typical linear and the sinusoidal TSFs is also included. The parameters of the adopted four phases machine are given in Table 1.

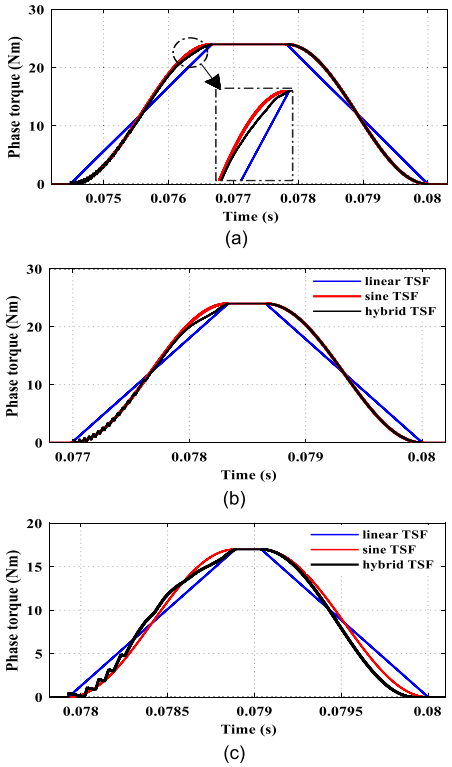

FIGURE 10. Reference torque profile at different operating points. (a) 750 r/min speed and 24 Nm torque. (b) 1500 r/min speed and 24 Nm torque. (c) 2250 r/min speed and 17 Nm torque.

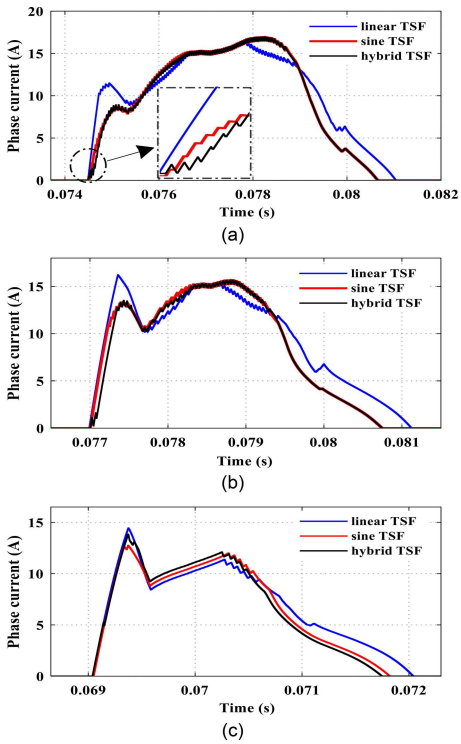

FIGURE 11. Actual phase currents of the SRM at different operating points. (a) 750 r/min speed and 24 Nm torque. (b) 1500 r/min speed and 24 Nm torque. (c) 2250 r/min speed and 17 Nm torque.

A typical hysteresis current regulator with a current band of 0.3A is utilized in this work. Fig. 8 depicts the

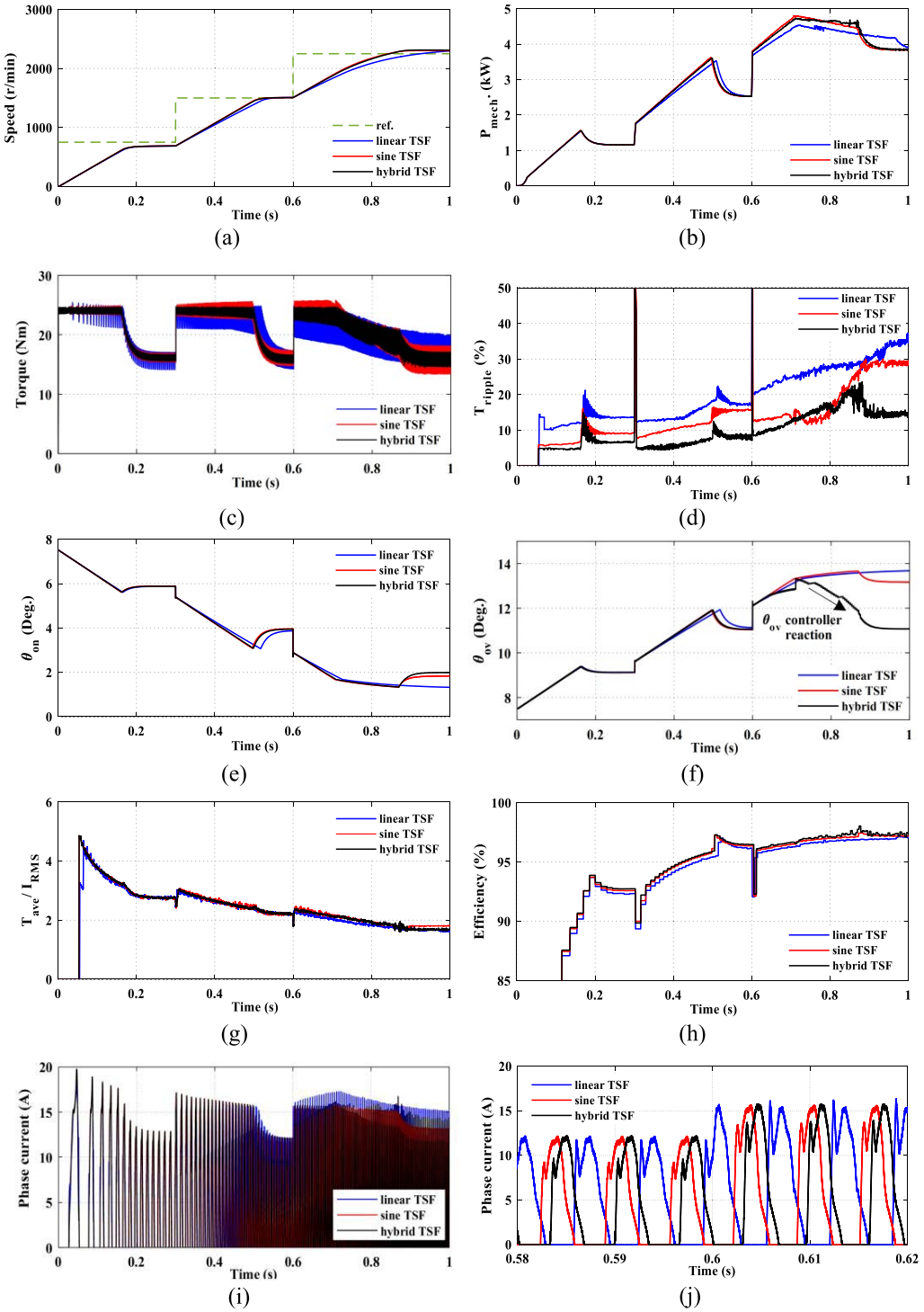

FIGURE 12. Dynamic performance of the SRM under speed changes responses. (a) Speed (r/min). (b) Output power (kW). (c) Torque profile (Nm). (d) Torque ripple percent. (e) Turn-on angle (Deg). (f) Overlap angle (Deg). (g) Torque/ampere ratio (Nm/A). (h) Efficiency (%). (i) Current of one phase (A). (j) A zoomed section of the phase current plot around the 0.6th second.

obtained performance indices when utilizing the linear, sinusoidal, and the proposed hybrid TSF over a wide speed range operation of the SRM. The turn-on angle is obtained from (16), and the same operating points are selected in all three methods. The performance indices include the average output torque (Fig. 8a), torque ripple percent (Fig. 8b), torque to current ratio (Fig.8 c), and the efficiency of the motor (Fig. 8d).

As illustrated, the hybrid TSF showed a notably higher average torque at very high speed, significant torque ripple reduction over the entire speed range, comparable torque/current ratio, and slightly higher efficiency. As a result, the

hybrid TSF provided overall enhanced performance over the traditional TSFs strategies.

Fig 9. depicts the torque profiles when operating the machine at low, medium, and high-speed commands (750, 1500, and 2250 r/min) at constant loads. As shown, the proposed hybrid TSF has the best torque profiles over the entire speed range.

Fig. 10. shows the reference torque profile of one phase of the SRM obtained from the linear, sinusoidal, and hybrid TSFs during on-line operation of the machine for the same operating points that have been utilized in Fig. 9. As it can be seen, the hybrid TSF modified the rising portion of phase torque profile to attain the exact mirroring of the declining part of the actual torque of the previous phases. As a result, the obtained torque profile in Fig. 9 is improved.

Fig. 11 shows the corresponding phase currents at the same operating points. The phase currents generated by the hybrid TSF have the optimal profile to keep the torque ripple to a minimum.

The dynamic performance of the machine is presented in Fig.12. The system is subjected to speed change commands from 750 to 1500 r/min and from 1500 to 2250 r/min, as depicted in Fig. 12a. The machine is loaded with a constant load torque of 16 Nm. The average output power is presented in Fig. 12b.

The torque profile is shown in Fig. 12c, and the corresponding torque ripple percent can be seen in Fig. 12d. The figures show that the hybrid TSF has the best dynamic torque profile with the lowest torque ripple.

The real-time variations of the turn-on angles seen in Fig. 12e are comparable. They correspond to the actual operating speed of the SRM and the commanded current value as indicated in (16).

The overlap angle variations are depicted in Fig. 12f. Initially, the overlap angle is set to the maximum limit (13) for best torque tracking accuracy, as illustrated in section V. However, after 0.7 sec, the overlap angle controller is involved since it starts to detect unacceptable torque error and, therefore, by modifying the overlap angle, higher torque tracking capability and thus, lower torque ripple is reached. Fig. 12g and 12h showed that the hybrid TSF has a comparable torque/current ratio and a bit higher efficiency than the typical linear and the sinusoidal TSFs. For clarity and simplification, only one phase current profile is given in Fig. 12i. A zoomed section of the current profile is also shown in Fig. 12j.

VII. CONCLUSION

This research presented a novel IITC system based on hybrid TSF for the SRMs. The main concern is to provide an enhanced torque profile with a lower torque ripple. The proposed hybrid TSF is created to solve the problem of the torque tracking error during phase demagnetization. Whereby re-profiling the reference torque portion of the incoming phase to be the exact mirroring of the actual torque of the outgoing phases, the problem can be solved, and the torque profile can be enhanced. Besides, within the proposed IITC system, an overlap angle controller is introduced to compensate for the error between the commanded and the average torque. The controller is mainly involved in high-speed operation.

Based on an accurate SRM model, a series of simulations are carried out, and the presented findings showed clear superiority over other typical TSF approaches.

REFERENCES

[1] B. Bilgin, J. W. Jiang, and A. Emadi, *Switched Reluctance Motor Drives*. Boca Raton, FL, USA: CRC Press, 2019.
[2] N. Zabihi and R. Gouws, "A review on switched reluctance machines for electric vehicles," in *Proc. IEEE 25th Int. Symp. Ind. Electron. (ISIE)*, Jun. 2016, pp. 799–804.
[3] Y. Lan, Y. Benomar, K. Deepak, A. Aksoz, M. E. Baghdadi, E. Bostanci, and O. Hegazy, "Switched reluctance motors and drive systems for electric vehicle powertrains: State of the art analysis and future trends," *Energies*, vol. 14, no. 8, p. 2079, Apr. 2021.
[4] E. Bostanci, M. Moallem, A. Parsapour, and B. Fahimi, "Opportunities and challenges of switched reluctance motor drives for electric propulsion: A comparative study," *IEEE Trans. Transport. Electrific.*, vol. 3, no. 1, pp. 58–75, Mar. 2017.
[5] P. Azer, B. Bilgin, and A. Emadi, "Mutually coupled switched reluctance motor: Fundamentals, control, modeling, state of the art review and future trends," *IEEE Access*, vol. 7, pp. 100099–100112, 2019.
[6] G. Watthewaduge, E. Sayed, A. Emadi, and B. Bilgin, "Electromagnetic modeling techniques for switched reluctance machines: State-of-the-art review," *IEEE Open J. Ind. Electron. Soc.*, vol. 1, pp. 218–234, 2020.
[7] S. J. Evangeline and S. S. Kumar, "Minimization of torque ripple in switched reluctance motor drive—A review," in *Advanced Electrical and Electronics Engineering* (Lecture Notes in Electrical Engineering), J. Lee, Ed. Berlin, Germany: Springer, 2011, pp. 287–294.
[8] S. Mapa and G. Bhuvaneswari, "A novel modeling approach for a switched reluctance machine for multi-quadrant operation," *Trans. Indian Nat. Acad. Eng.*, vol. 5, no. 4, pp. 629–641, Nov. 2020.
[9] V. Dmitrievskii, V. Prakht, and V. Kazakbaev, "Novel rotor design for high-speed flux reversal motor," *Energy Rep.*, vol. 6, pp. 1544–1549, Dec. 2020.
[10] E. F. I. Raj, M. Appadurai, E. F. I. Rani, and I. Jenish, "Finite-element design and analysis of switched reluctance motor for automobile applications," *Multiscale Multidisciplinary Model., Exp. Des.*, vol. 5, no. 3, pp. 269–277, Jan. 2022.
[11] J. Lee, J. H. Seo, and N. Kikuchi, "Topology optimization of switched reluctance motors for the desired torque profile," *Struct. Multidisciplinary Optim.*, vol. 42, no. 5, pp. 783–796, 2010.
[12] G. Guidkaya, E. D. K. Fankem, and J. Y. Effa, "A new rotor shape design of 6/2 switched reluctance motor: Comparative analysis of its chaotic behavior with other structures," *J. Electr. Eng. Technol.*, vol. 16, no. 1, pp. 309–320, Oct. 2020.
[13] A. Peniak, J. Makarovic, P. Rafajdus, V. Vavrus, P. Makys, K. Buhr, and R. Fajtl, "Design and optimization of switched reluctance motor for electrical vehicles," *Electr. Eng.*, vol. 99, no. 4, pp. 1393–1401, Jul. 2017.
[14] M. Deepak, G. Janaki, and J. Mounica, "Investigation on airgap selection for switched reluctance motor on low power electric vehicles," *Mater. Today, Proc.*, vol. 64, pp. 255–260, Apr. 2022.
[15] R. Abdel-Fadil, F. Al-Amyal, and L. Szamel, "Torque ripples minimization strategies of switched reluctance motor—A review," in *Proc. Int. IEEE Conf. Workshop Óbuda Electr. Power Eng. (CANDO-EPE)*, Nov. 2019, pp. 41–46.
[16] C. Gan, J. Wu, Q. Sun, W. Kong, H. Li, and Y. Hu, "A review on machine topologies and control techniques for low-noise switched reluctance motors in electric vehicle applications," *IEEE Access*, vol. 6, pp. 31430–31443, 2018.
[17] G. Fang, F. P. Scalcon, D. Xiao, R. Vieira, H. Grundling, and A. Emadi, "Advanced control of switched reluctance motors (SRMs): A review on current regulation, torque control and vibration suppression," *IEEE Open J. Ind. Electron. Soc.*, vol. 2, pp. 280–301, 2021.
[18] S. Dhale, B. Nahid-Mobarakeh, and A. Emadi, "A review of fixed switching frequency current control techniques for switched reluctance machines," *IEEE Access*, vol. 9, pp. 39375–39391, 2021.
[19] D. F. Valencia, R. Tarvirdilu-Asl, C. Garcia, J. Rodriguez, and A. Emadi, "A review of predictive control techniques for switched reluctance machine drives. Part II: Torque control, assessment and challenges," *IEEE Trans. Energy Convers.*, vol. 36, no. 2, pp. 1323–1335, Jun. 2021.

[20] F. Al-Amyal and L. Számel, "Analytical approach for the turn-off angle in switched reluctance motors," in *Proc. 6th Int. Congr. Inf. Commun. Technol.* (Lecture Notes in Networks and Systems), vol. 217. Singapore: Springer, pp. 685–696, 2022.
[21] P. Bober and Ž. Ferková, "Firing angle adjustment for switched reluctance motor efficiency increasing based on measured and simulated data," *Electr. Eng.*, vol. 104, no. 1, pp. 191–202, Jun. 2021.
[22] B. Anvari, H. A. Toliyat, and B. Fahimi, "Simultaneous optimization of geometry and firing angles for in-wheel switched reluctance motor drive," *IEEE Trans. Transport. Electrific.*, vol. 4, no. 1, pp. 322–329, Mar. 2018.
[23] A. Shahabi, A. Rashidi, M. Afshoon, and S. M. S. Nejad, "Commutation angles adjustment in SRM drives to reduce torque ripple below the motor base speed," *Turkish J. Electr. Eng. Comput. Sci.*, vol. 24, no. 2, pp. 669–682, 2016.
[24] F. Al-Amyal, M. Hamouda, and L. Számel, "Torque quality improvement of switched reluctance motor using ant colony algorithm," *Acta Polytechnica Hungarica*, vol. 18, no. 7, pp. 129–150, 2021.
[25] M. Debouza, A. Al-Durra, H. M. Hasanien, S. Leng, and W. Taha, "Optimization of switched reluctance motor drive firing angles using grey wolf optimizer for torque ripples minimization," in *Proc. IECON 44th Annu. Conf. IEEE Ind. Electron. Soc.*, Oct. 2018, pp. 619–624.
[26] M. Hamouda, A. A. Menaem, H. Rezk, M. N. Ibrahim, and L. Számel, "Numerical estimation of switched reluctance motor excitation parameters based on a simplified structure average torque control strategy for electric vehicles," *Mathematics*, vol. 8, no. 8, p. 1213, Jul. 2020.
[27] G. Fang and J. Bauman, "Optimized switching angle-based torque control of switched reluctance machines for electric vehicles," in *Proc. IEEE Transport. Electrific. Conf. Expo (ITEC)*, Jun. 2020, pp. 186–191.
[28] M. U. Jamil, W. Kongprawechnon, and N. Chayopitak, "Average torque control of a switched reluctance motor drive for light electric vehicle applications," *IFAC-PapersOnLine*, vol. 50, no. 1, pp. 11535–11540, Jul. 2017.
[29] J. Fan and Y. Lee, "A novel average torque control of switched reluctance motor based on flux-current locus control," *Can. J. Electr. Comput. Eng.*, vol. 43, no. 4, pp. 273–281, 2020.
[30] A. Pillai, A. S. K. V. Gangadharan, P. Umesht, and S. Bhaktha, "Modeling and analysis of average torque control strategy on switched reluctance motor for e-mobility," in *Proc. IEEE Int. Conf. Electron., Comput. Commun. Technol. (CONECCT)*, Jul. 2021, pp. 1–6.
[31] M. Hamouda, A. A. Menaem, H. Rezk, M. N. Ibrahim, and L. Számel, "Comparative evaluation for an improved direct instantaneous torque control strategy of switched reluctance motor drives for electric vehicles," *Mathematics*, vol. 9, no. 4, p. 302, Feb. 2021.
[32] Y. Cheng, "Modified PWM direct instantaneous torque control system for SRM," *Math. Problems Eng.*, vol. 2021, pp. 1–13, Oct. 2021.
[33] F. Al-Amyal, M. Hamouda, and L. Számel, "Performance improvement based on adaptive commutation strategy for switched reluctance motors using direct torque control," *Alexandria Eng. J.*, vol. 61, no. 11, pp. 9219–9233, Nov. 2022.
[34] N. Yan, X. Cao, and Z. Deng, "Direct torque control for switched reluctance motor to obtain high torque–ampere ratio," *IEEE Trans. Ind. Electron.*, vol. 66, no. 7, pp. 5144–5152, Jul. 2019.
[35] S. Wang, Z. Hu, and X. Cui, "Research on novel direct instantaneous torque control strategy for switched reluctance motor," *IEEE Access*, vol. 8, pp. 66910–66916, 2020.
[36] X. D. Xue, K. W. E. Cheng, and S. L. Ho, "Optimization and evaluation of torque-sharing functions for torque ripple minimization in switched reluctance motor drives," *IEEE Trans. Power Electron.*, vol. 24, no. 9, pp. 2076–2090, Sep. 2009.
[37] J. Ye, B. Bilgin, and A. Emadi, "An offline torque sharing function for torque ripple reduction in switched reluctance motor drives," *IEEE Trans. Energy Convers.*, vol. 30, no. 2, pp. 726–735, Jun. 2015.
[38] C. Li, C. Zhang, J. Liu, and D. Bian, "A high-performance indirect torque control strategy for switched reluctance motor drives," *Math. Problems Eng.*, vol. 2021, pp. 1–15, Feb. 2021.
[39] Z. Xia, B. Bilgin, S. Nalakath, and A. Emadi, "A new torque sharing function method for switched reluctance machines with lower current tracking error," *IEEE Trans. Ind. Electron.*, vol. 68, no. 11, pp. 10612–10622, Nov. 2021.
[40] A. K. Rana and A. V. Raviteja, "A mathematical torque ripple minimization technique based on a nonlinear modulating factor for switched reluctance motor drives," *IEEE Trans. Ind. Electron.*, vol. 69, no. 2, pp. 1356–1366, Feb. 2022.
[41] F. Al-Amyal, L. Al Quraan, and L. Szamel, "Torque sharing function optimization for extended speed range control in switched reluctance motor drive," in *Proc. IEEE 3rd Int. Conf. Workshop Óbuda Electr. Power Eng. (CANDO-EPE)*, Nov. 2020, pp. 119–124.
[42] M. Hamouda, A. A. Menaem, H. Rezk, M. N. Ibrahim, and L. Számel, "An improved indirect instantaneous torque control strategy of switched reluctance motor drives for light electric vehicles," *Energy Rep.*, vol. 6, pp. 709–715, Dec. 2020.
[43] M. Hamouda and L. Számel, "Accurate magnetic characterization based model development for switched reluctance machine," *Periodica Polytechnica Electr. Eng. Comput. Sci.*, vol. 63, no. 3, pp. 202–212, Jun. 2019.
[44] M. Hamouda and L. Számel, "A new technique for optimum excitation of switched reluctance motor drives over a wide speed range," *Turkish J. Electr. Eng. Comput. Sci.*, vol. 26, no. 5, pp. 2753–2767, Sep. 2018.

FAHAD AL-AMYAL received the B.S. degree in electrical engineering from the University of Kufa, Najaf, Iraq, in 2010, and the M.S. degree in electrical engineering from Baghdad University, Baghdad, Iraq, in 2013. He is currently pursuing the Ph.D. degree in electrical engineering with the Budapest University of Technology and Economics.

His research interests include electric motor drives, power electronics, and electric vehicles.

LÁSZLÓ SZÁMEL received the M.S. and Ph.D. degrees in electrical engineering from the Technical University of Budapest, in 1995 and 2005, respectively.

Until 1997, he worked with the Computer and Automation Research Institute, Hungarian Academy of Sciences. He is currently an Associate Professor with the Department of Electric Power Engineering, Budapest University of Technology and Economics. His research interests include electrical drive control, servo and robot drives, digital systems, switched reluctance motor drives, and high-accuracy position and speed measurements of electrical drives. He is a member of the Hungarian Electrotechnical Association.